Construction and Building Materials 188 (2018) 326–336

Contents lists available at ScienceDirect

Construction and Building Materials

journal homepage: www.elsevier.com/locate/conbuildmat

Long-term curing impact on properties, mineral composition and microstructure of hemp shive-cement composite

Giedrius Balčiūnas [a,*], Ina Pundienė [b], Renata Boris [c], Agnė Kairytė [a], Jadvyga Žvironaitė [b], Justinas Gargasas [d]

[a] Vilnius Gediminas Technical University, Institute of Building Materials, Laboratory of Thermal Insulating Materials and Acoustics, Linkmenų St. 28, 08217 Vilnius, Lithuania
[b] Vilnius Gediminas Technical University, Institute of Building Materials, Laboratory of Concrete Technologies, Linkmenų St. 28, 08217 Vilnius, Lithuania
[c] Vilnius Gediminas Technical University, Institute of Building Materials, Laboratory of Composite Materials, Linkmenų St. 28, 08217 Vilnius, Lithuania
[d] Vilnius Gediminas Technical University, Faculty of Mechanics, Department of Mechanical and Material Engineering, J. Basanavičiaus St. 28, 03224 Vilnius, Lithuania

HIGHLIGHTS

- Mechanical properties of composite during long-term hardening period increase.
- Changes of properties are caused by continuing hydration and carbonation processess.
- Hydration and carbonisation depends from $Al_2(SO_4)_3$ and $Ca(OH)_2$ ratio with cement.
- Qualitative analysis of the composite composition is conducted using X-ray and DTA.

ARTICLE INFO

Article history:
Received 19 January 2018
Received in revised form 12 June 2018
Accepted 19 August 2018
Available online 24 August 2018

Keywords:
Hemp shiv
Cement
Composite
Long-term properties
X-ray analysis
Mineralization

ABSTRACT

Fibre Hemp Shiv (FHS) is one of the most widely used bio-aggregates for the development of eco-friendly building materials. Research on composites with an FHS aggregate has usually been limited to short-term property analyses that depend on the type of binder. Such properties are determined after (7–90) days of curing. Most scientists have focused on researching composites with lime (L) based binders. This work focuses on composites with a cement (CEM) binder and FHS aggregate, and investigates the impact of long-term curing (for 1 year) on the physical properties (density, compressive strength and thermal conductivity) of composites with non-treated and mineralized FHS (mineralization is performed with aluminium sulphate (AS) and hydrated lime (L)). In order to determine the causes of the changes in properties during long-term curing, changes in the mineralogical composition are analysed. X-ray diffraction, differential thermal and thermogravimetric analyses as well as research on the microstructure of the composites are implemented. The lowest change in properties due to inhibition of hydration is determined for composites with a non-treated aggregate.

Mineralized aggregates are characterized by lower cement hydration capability over a long-term period. The change of properties after 1 year of curing depends on the AS/CEM ratio. For all 1-year cured composites, there is a reduction in the peak intensities of C_2S, C_3S and ettringite, whereas there is an increase in the peak intensities of calcite, (except for composition with the highest AS/CEM ratio – AS30L18), Calcium Silicate Hydrate (CSH) and portlandite (except for the non-mineralized composition). Lower ratios for AS/CEM (AS18L36 and AS21L42) and, respectively, higher L/CEM ratios in compositions lead to the formation of vaterite. In addition, the above-mentioned composition has the highest L/CEM ratio, which ensures that more hydrates participate in the carbonation process, thus leading to higher compressive strength, denser composite structure and higher thermal conductivity due to higher heat transfer by conduction.

1. Introduction

Fibre Hemp Shiv (FHS) is generally considered as a by-product of long fibre and seed production [1]. FHS has a porous microstruc-

Abbreviations: CEM, cement; FHS, Fibre Hemp Shiv; AS, aluminium sulphate; CM, complex mineralizer; CSH, Calcium Silicate Hydrate; DTA, differential thermal analysis; TG, thermogravimetry; L, lime; SP, superplasticizer.

* Corresponding author.
E-mail address: giedrius.balciunas@vgtu.lt (G. Balčiūnas).

https://doi.org/10.1016/j.conbuildmat.2018.08.126
0950-0618/

ture [2] that determines the suitability of the material to be used as an aggregate for light-weight concretes. The production of the usual low-weight aggregates used in the production of low-density concretes requires high temperature processing. For example, production of expanded clay aggregates is carried out by heating clay to around 1200 °C; foam glass lightweight aggregate production goes in at about 800 °C. It is understandable that production at such high temperatures leads to high energy consumption. In addition, in the case of expanded clay concrete production, Aeratet Autoclaved concrete production fossil raw materials are used, the amount of which is finite. FHS aggregates, on the other hand, have a great advantages: the porous microstructure of the aggregate is created by nature; fossil raw materials are avoided because FHS is a renewable resource, and hemp plant cultivation leads to CO_2 absorption via photosynthesis. While the energy efficiency requirements for buildings are becoming stricter, light-weight concretes become more useful for the installation of bearing structures in low-rise or multi-storey buildings, and the ecology aspect is taken into consideration due to human needs for environmental cleanliness and ecology. In order to develop environmentally friendly, energy efficient materials at a competitive price, it is advantageous to relate the agriculture and building industries [3]. FHS with an L-based binder is widely used in the construction sector as an aggregate for the production of hemp concrete that can be used for renovating old building envelopes or installing new ones (insulation of walls, ground and roof) [2,4]. The main advantages of hemp concrete with an L binder are sufficient thermal insulating and acoustic properties [5,8,9], low environmental impact [6], and buffer moisture properties [7]. However, their mechanical properties are rather low (up to 1 MPa) [10]. Such compressive strength is insufficient for the installation of load-bearing structures. Higher compressive strength may be obtained for hemp concrete when Portland cement is used. In this case, a mineralization process is necessary for the aggregates. With proper treatment (with AS and L) of the FHS aggregate, a compressive strength of up to 8 times higher than that of a composite without mineralized aggregates may be obtained [14]. High effectiveness of mineralisation with AS and L was also demonstrated by Thai researchers [49], who found that compressive strength can be improved up to 4 times. The above-mentioned authors also highlight that different amounts of AS and L in various compositions have minimal influence on hemp-concrete properties, and improved compressive strength can be obtained by using only AS. Mineralization of FHS aggregates is a process that neutralizes compounds harmful to cement hydration, such as saccharides, fatty acids etc. [11]. Such materials mostly consist of the following groups: terpenes, fatty acids, tannins and inorganic materials [11,12]. It is determined that acidic tannin derivatives (sugar acids, gallic acids, ellagic acids) inhibit cement-binding behaviour and reduce the strength of cement stone [15,16]. Water-soluble materials have the greatest inhibiting effect [17]. Their compounds have HO–C–H groups that are considered as groups actively impeding the cement hydration process. HO–C–H groups are absorbed on the surfaces of tricalcium aluminate (C_3A) and tricalcium silicate (C_3S), thus forming a layer on the cement grain that interferes with the penetration of water. OH groups existing in carboxy acids are also considered as adsorption groups. The hydration of C_3A is strongly inhibited by organic impurities. These impurities have an impact on the nucleation of calcium hydroxide during the hydration reaction of C_3S, and also determine the prolonged period of the hydration inactivity state. Gluconates impede the hydration of all cement phases [18]. Scientists [19] state that, in an alkali medium, AS is suitable for the saturation of plant-based aggregates due to the formation of water insoluble $Al(OH)_3$ compounds (reaction 1) that fill the pores and gaps:

$$Al_2(SO_4)_{3(aq)} + 6OH^-_{(aq)} = 2Al(OH)_{3(s)} + 3SO^{2-}_{4\,(aq)} \quad (1)$$

Treatment with AS not only helps to avoid harmful effects on hydration, but also the resulting $Al(OH)_3$ increases fire resistance because its decomposition temperature is approximately (210–300)°C [20]. Some authors have dealt with the impact of L treated hemp on the mechanical properties of hemp concrete. Hemp fibres fix calcium ions on their surface probably through the formation of a stable calcium–pectin complex [21]. It is worth mentioning that the treatment of plant-based aggregates with L is not suitable for all mineral binders. Scientists have found a decrease in the compressive strength of a composite with an MgO cement binder using L-treated hemp shiv [22]. One study [23] analyses a similar concrete with plant-based aggregates, such as rice husk treated with a lime solution. In this case, the treatment improved the compressive strength of the final concrete, but no characterization of rice husks after this treatment was provided in order to explain these results. When L is used as an eco-friendly binder, carbonation contributes towards strength as the plant-based concrete ages [24].

Frequently, the compressive strength of traditional concretes and previously tested FHS-cement composites [14] is determined after 28 days of hardening, however, building structures are exploited over the long-term (the design working life for buildings is 50 years [25], and the hardening process is still in progress). Although the literature widely analyses the hydration processes for traditional concretes [26,27], there is no thorough analysis of light-weight concretes from mineralized plant-based aggregates. Therefore, the impact of the component (AS and L in different ratios) used for the mineralization of FHS on the long-term hydration of cement is not clear.

The main aim of this paper is to analyse the long-term curing impact on a composite made from mineralized hemp shive with a cement binder, as regards its properties, mineralogical composition and microstructure. The main objectives of this article are to compare the physical and mechanical properties, mineral composition and microstructure of composites with a cement binder and mineralized FHS aggregates cured over 28 days and approximately 1 year respectively. In order to justify the results of X-ray diffraction analysis, thermogravimetric (TG) and differential thermal analyses are carried out.

2. Materials and methods

2.1. Raw materials

Hemp shiv aggregate is obtained from hemp (variety USO 31) grown in Eastern Lithuania and used as an aggregate. FHS with a size of (2.5–10) mm is used. The bulk density is 105 kg/m^3. The chemical composition of FHS is presented in Table 1.

Table 1
Chemical composition of FHS.

Raw material	Cellulose	Lignin	Extractives	Ash	Hemicellulose	Pectins
	%					
Hemp stalks	46.9	17.4	1.9	1.3	24.6	7.9

CEM I 52.5 R cement (CEM) according to EN 197-1 is used as a binder. The chemical composition of the cement, wt. %, is as follows: CaO – 64.02, SiO_2 – 20.09, Al_2O_3 – 4.84, Fe_2O_3 – 3.87, SO_3 – 2.83, free CaO – 4.35, and the mineralogical composition, wt. %: C_3S – 65.8, C_2S – 11.8, C_3A – 5.2, C_4AF – 7.8.

A complex mineralizer (CM) consisting of $Al_2(SO_4)_3{\cdot}18H_2O$ (AS) (pH 3.5) and hydrated lime (L) (particle surface area estimated by Blaine method is 618 m^2/kg) is used for FHS mineralization. Polycarboxylate ether-based superplasticizer (SP) Glenium 430 is used for enhancing the rheological properties of the formation mixture and the mechanical properties of the composite.

2.2. Composition and formation methodology

Preparation of the forming mixture was carried out using a 5 l rotary mixer. The formation process of composites consists of two stages – mineralization of the aggregates and preparation of the forming mixture. Mineralization of the aggregates was carried out according to the technology developed in Bialystok University [13], which, in previous research [14], was adapted for FHS mineralization. $Al_2(SO_4)_3$ and hydrated lime $Ca(OH)_2$ were dissolved in mixing water divided into two equal parts (the total water amount for the mineralization process was $1.5{\cdot}m_{FHS}$, where m_{FHS} – mass of hemp shiv aggregate). First, the organic aggregate was mixed with AS solution for 3 min until homogeneous saturation. After waiting 15 min, L was added, and all components were mixed again for 1 min. The remaining amount of water was mixed with plasticizer and cement. The cement paste obtained was added to the mineralized FHS. A control sample was formed using the same forming technology, except that the treatment of the organic aggregate was carried out not with the AS solution but only with water. The compositions of the forming mixtures are presented in Table 2.

For all compositions, the amount of SP was calculated as 0.9% by cement mass C, W/C ratio – 0.32, FHS/C ratio – 0.25. Long-term tests were conducted on four different compositions that had been hardened for 1 year: the control sample (with non-mineralized FHS); a composition with mineralized FHS, using a higher amount of AS for mineralisation compared to L (AS30L18); the composite which had the greatest compressive strength after 28 days (AS18L36) and the composite with a higher amount of overall mineralizer (AS21L42).

2.3. Test methods

Specimens for all test methods were stored at (22 ± 2) °C and (50 ± 5) % RH. For the density and compressive strength tests, the conditioning conditions for the specimens were the same as the storage conditions. For the thermal conductivity test, specimens were dried at (100 ± 5)°C under constant mass before the test, and then cooled to room temperature in a closed bag. The specimens were tested after 28 days and 1 year of storage respectively. The compressive strength of the composites was determined according to the requirements of EN 772-1 using a Tinius Olsen H200 KU laboratory pressing machine with maximum loading – 200 kN, loading accuracy ±0.5%, positioning accuracy – ±0.01%, and loading speed – 0.05 (N/mm^2)/s. 5 specimens (100 × 100 × 100 mm) of each composition were tested.

Thermal conductivity tests were performed using a FOX 304 (LaserComp, USA) heat-flow meter apparatus. The measurement range of the apparatus was from 0.5 W/(m·K) to 0.004 W/(m·K) with centrally located heat flux transducers having dimensions of (100 × 100) mm. The thermal insulating properties of the materials were measured in accordance with EN 12664 and ISO 8301. 3 specimens (300 × 300 × 50 mm) of each composition were tested. Measurements were carried out at an average temperature of 10 °C (upper plate of the apparatus maintains a temperature of 0 °C and the lower plate 20 °C). Specimens before the test were dried at (70 ± 2)°C under constant mass, and then cooled to room temperature in a closed bag.

The microstructure of the composites was explored with an "FEI Helios NanoLab 650"scanning electron microscope, resolution – 0.8 nm. Before the tests, the specimen surfaces were coated with a layer of gold; the accelerating voltage used during the test was 20 kV.

X-Ray diffraction (XRD) analysis was conducted using a SmartLab (Rigaku) X-ray diffractometer with a 9 kW rotating anode Cu X-ray tube (λ = 0.15418 nm). The XRD patterns were measured using Bragg-Brentano geometry with a bent graphite monochromator in the path of the diffracted beam. A high temperature stage DHS 1100 (Anton Paar) was used. The quantitative change of minerals in the XRD patterns was evaluated according to the heights of the main diffraction peaks.

TG/DTA curves were registered with a Linseis STA PT-1600 thermal analytical instrument up to 1000 °C (with a temperature rise rate of 10 °C/min; air was used as the heating environment; the weight of the specimens was (50 ± 5) mg).

Table 2
Composition of the forming mixtures.

Codes of composites	AS/L ratio	AS/CEM ratio	L/CEM ratio
Control	–	–	–
AS18L36	1:2	1:0.045	1:0.09
AS21L42	1:2	1:0.053	1:0.11
AS30L18	1:0.59	1:0.075	1:0.045

AS – $Al_2(SO_4)_3$; L – hydrated lime; CEM – cement.

3. Results and discussion

3.1. X-ray diffraction analysis

The changes in the properties of the FHS and cement composites occur due to long-term carbonation and hydration processes or polymorphic transformations during cement matrix curing. X-ray diffraction patterns of the control (not mineralized) specimens after 28-days and 1-year of curing respectively are presented in Fig. 1.

In the control specimen without CM, diffraction peaks of portlandite (P), which is the main component of hydration products, are not identified after 28 days. Non-reacted cement minerals C_3S and C_2S, ettringite (E), calcite (C) and small amount of CSH are found. Usually, C_3S and C_2S undergo hydration to form P and CSH, which is the principal contributor to cement strength [28]. However, materials harmful to cement hardening, which can be found in plant-based aggregates, impede cement hydration. A very small amount of sugars may considerably impede the hydration of cement. Scientists [29] have determined that the addition of 0.15 wt% of sucrose to C_3S paste prevented hydration for 56 days, and completely eliminates the appearance of CSH. In the presence of sugars, the single-phase hydration of cement is different [31,15]. CSH forms in very small amounts in the shape of fine derivatives. During the interaction of sugars with C_3A, the formation of the hexagonal phase C_4AH_{13} is promoted instead of the cubic phase C_3AH_6, and this retards gypsum consumption as well as the formation of E and monosulphate [30]. However, other scientists [32] specify that, in the presence of sucrose, C_3A reacts directly with gypsum to form E and the reaction rate is significantly increased.

When the composition contains FHS, the silica concentration in the cement paste increases because it cannot precipitate with calcium to form CSH [35]. Sugars, which can trap calcium, act as a

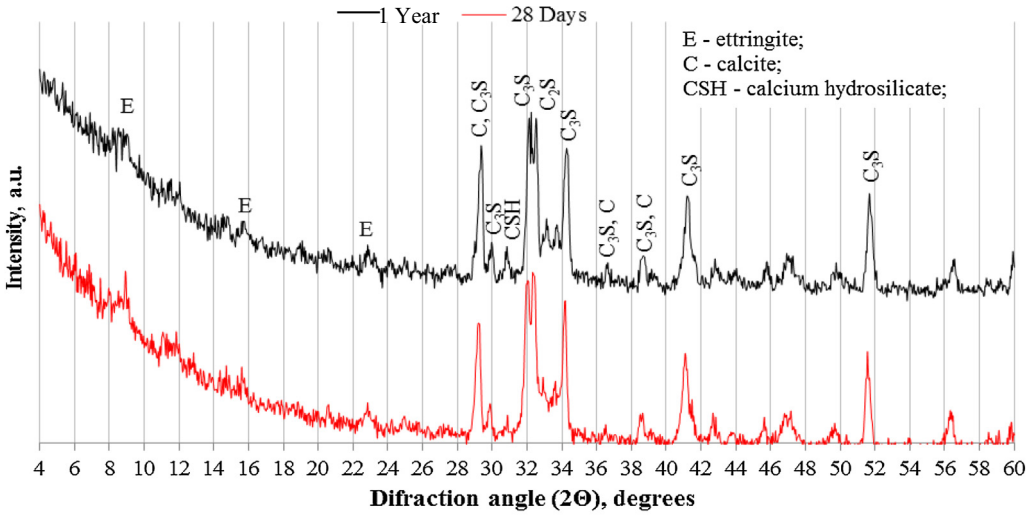

Fig. 1. XRD of control specimens after 28-days and 1-year of curing.

growth inhibitor for CSH hydrates. FHS should induce the same process because their chemical composition is close to the chemical composition of hemp. However, the very small amounts of CSH observed show that minimum hydration processes of cement minerals have taken place. Therefore, as C_2S hydrates slower than C_3S [35], it may be assumed that CSH is formed under hydration from the former. Moreover, according to SEM investigation [17], C_3S particles are covered by flaky CSH, thus poisoning the stable CSH nuclei when sugars are present [31].

After 1 year, a lower amount of E is detected in the control specimens. E is not stable without protective C-S-H gel layers [37] and can slowly dissolve and reform in any available voids or micro cracks as well as convert to calcium aluminate monosulphate and other mineral forms [37]. Based on the above-mentioned studies, it may be concluded that the observed reduction of E is due to the very small amount of CSH. Comparing the intensities of the peaks of C after 28 days, it can be seen that after 1 year the intensity is increased by approximately (10–15)%. In conditions of humidity and temperature, CO_2 diffuses into a composite and reacts with free $Ca(OH)_2$. Under usual positive air temperature, favourable air humidity for carbonation is (50–60)% [38].

28-day and 1-year X-ray patterns of AS18L36 composition are presented in Fig. 2.

Besides E, C and CSH, P can be identified in 28-day specimens AS18L36 with the lowest AS/CEM ratio. During previous studies [15], it was determined that part of the Ca ions from CM bond with FHS. Unreacted Ca ions from the mineralization reaction participate in the hydration reaction and more P forms. This is confirmed by the higher diffraction peaks of P, E and CSH. The fact that AS has an effect on the stimulation and formation of E is stated in [35,49]. Cement minerals hydrate more actively, which is proved by the non-reacted C_3S and C_2S diffraction peaks that are considerably lower (approx. 20%) compared to the control specimen.

A newly formed mineral – vaterite (V) – a metastable phase of calcium carbonate, is observed in specimens after 1 year of curing. Therefore, once V is exposed to water, it transforms to C (at low temperature) or aragonite (at high temperature: ~60 °C) [39]. V formation is basically determined by $Ca(OH)_2$, which gets into the composite matrix in two ways: as a hydration product – P and as one of the components of CM. The impact of moisture is an additional factor for V occurrence. It is assumed that moisture migrates through the specimen due to the hygroscopicity of FHS,

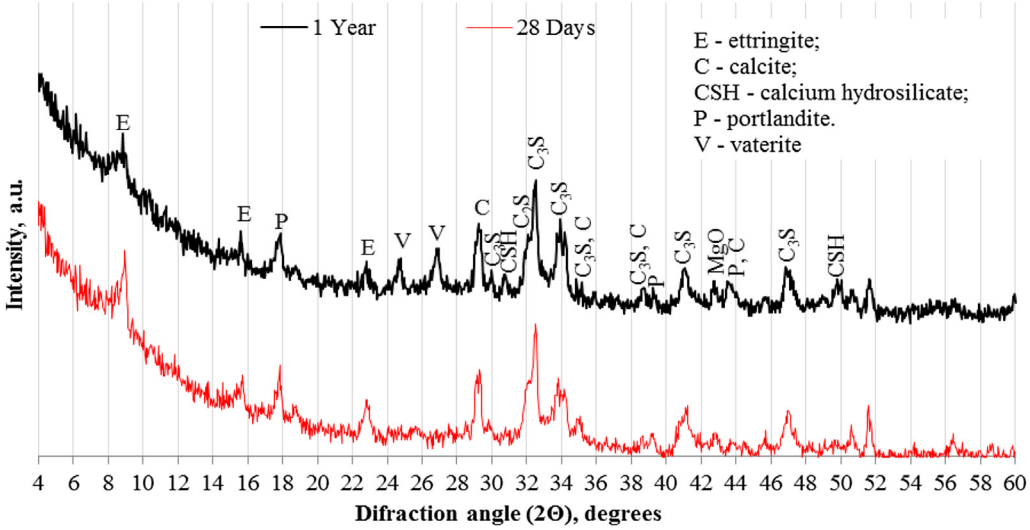

Fig. 2. XRD of AS18L36 specimens after 28-days and 1-year of curing respectively.

which absorbs moisture from the environment, and thus V forms over a long-term period.

After 1 year, the intensity of the diffraction peaks of E and P is reduced by approximately 10% but remains significantly higher than those in the control specimen. During the year, the P/E ratio changes from 0.57 to 0.63. As expected, the intensity of CSH diffraction peaks increases. The reduction in the intensity of the C diffraction peaks and V occurrence shows that the hydration process (when FHS are mineralized) proceeds differently compared to the control specimen.

28-day and 1-year X-ray patterns of AS21L42 composition are presented in Fig. 3.

XRD of the AS21L42 specimen shows similar tendencies as in the case of AS18L36 with the lowest AS/ CEM, and the same minerals can be observed after 28 days. For the AS21L42 specimen, it may be seen that the diffraction peak intensities of E are lower by (7–8) % in comparison to those of the AS18L36 specimen. This is can also be seen from the lower P/E ratio (0.47). Despite the fact that the AS and L ratio in CM is the same, the amount of CM in the AS21L42 specimen is approx. 20% higher compared to that of the AS18L36 specimen. AS is an acidic component and if its amount is low [36], the formation of E is accelerated, because the formation process is highly dependent on pH [38]. When the pH of the solution reduces, the formation of E is inhibited.

In 1-year AS21L42 specimens, V diffraction peaks are seen, and the intensities of the diffraction peaks of C, E, C_3S and C_2S are noticeably reduced compared to the intensities of the 28-day specimen. Peak growth of P and CSH may be observed (up to 5%). During the year, the P/E ratio rises to 0.56, but this ratio is less than in the AS18L36 sample after 28 days. After 1 year of curing, a general reduction tendency of C_2S and C_3S peaks is noticed under the formation of P, V, C and CSH in both specimens AS18L36 and AS21L42.

28-day and 1-year X-ray patterns of the AS30L18 composition are presented in Fig. 4.

When the AS/CEM ratio and the AS/L ratio of CM is the highest, changes in the mineralogy of AS30L18 specimens are also observed. In XRD of the 28-day specimen, the existence of C_3S, C_2S, E, P, CSH and C diffraction peaks is visible. The highest peak intensity of E is observed, and this is probably obtained due to the highest AS/CEM and AS/L ratio; a small amount of P is formed as well. In the above-mentioned composition, the P/E ratio is the lowest (0.29). After 1 year, the intensity of the E peak reduces, but a considerable increase in the intensities of the P peak can be observed, which is why the P/E ratio rises to 1.02. One more

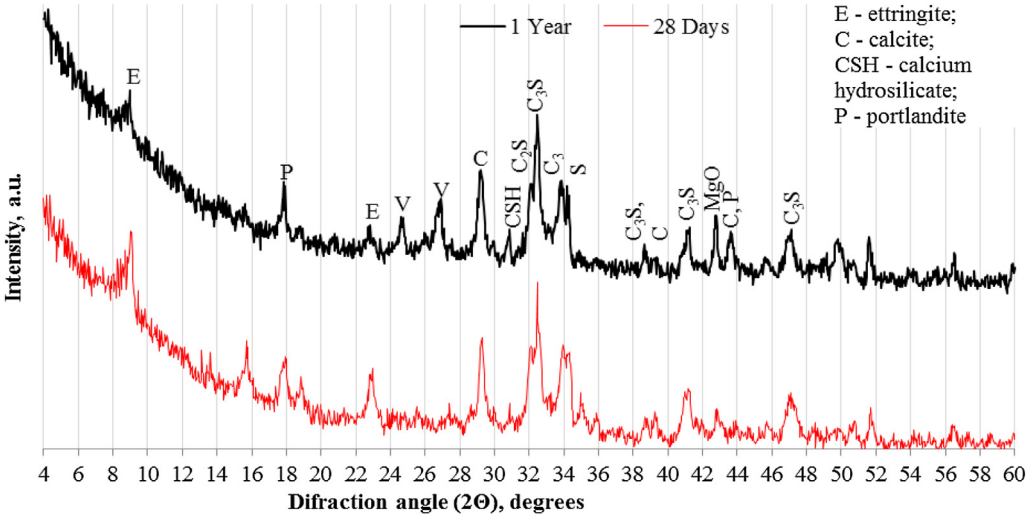

Fig. 3. XRD of AS21L42 specimens after 28-days and 1-year of curing respectively.

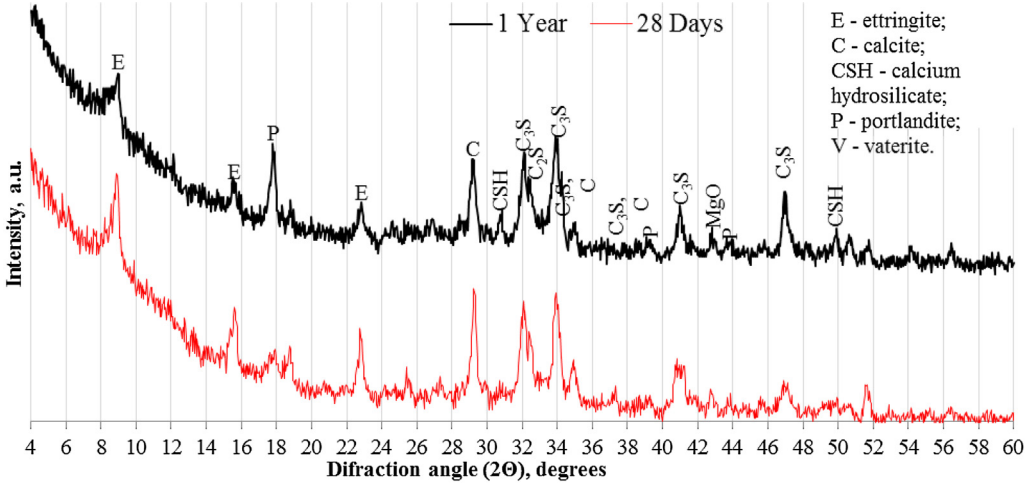

Fig. 4. XRD of AS30L18 specimens after 28-days and 1-year of curing respectively.

Table 3
Diffraction peaks (arbitrary units) for specimens of 28-days and 1-year.

	Control		AS18L36		AS21L42		AS30L18	
	28 days	1 year	28 days	1 year	28 days	1 year	28 days	1 year
Ettringite 2θ ≈ 9.0°	275.0	267.0	318.0	293.5	345.5	312.5	456.5	210.0
Portlandite 2θ ≈ 18.0°	–	–	181.5	185.0	164.0	175.5	132.0	215.0
Vaterite 2θ ≈ 26.8°	–	–	–	148.5	–	157.0	–	–
Calcite 2θ ≈ 29.2°	225.0	245.0	175.0	184.0	187.0	195.0	224.5	195.0
C_3S 2θ ≈ 32.3°	282.0	273.0	246.5	231.5	255.5	263.5	169.0	149.0
C_2S 2θ ≈ 32.0°	274.0	263.0	171.0	163.0	177.5	177.5	208.5	195.0
CSH 2θ ≈ 49.80°	81.0	110.2	105.1	124.4	103.2	127.7	90.0	117.1
P/E	0	0	0.57	0.63	0.47	0.56	0.29	1.02

important difference – no V peaks occur in the specimen. Apparently, at a higher amount of AS, more favourable conditions are obtained for calcium ions to participate in the formation of P compared to the carbonation process, which reduces. Table 3 presents the intensities of the diffraction peaks for 28-day and 1-year specimens.

3.2. DTA and TG of 28-day and 1-year composites

Differential thermal (DTA) analysis together with thermogravimetric (TG) analysis helps to evaluate whether the XRD analysis is correct. DTA and TG curves are presented in Figs. 5 and 6.

The decomposition of a pure FHS sample consists of 3 exothermal effects such as hemicellulose at (260–300) °C, cellulose at (300–340) °C and lignin at (400–440) °C (Fig. 5). Mass losses of the FHS specimen up to 260 °C is 10%, on an interval of 260–340 °C – 60% and 14% on an interval of 240–350 °C.

The decomposition process of wood (under vacuum) during pyrolysis differs from decomposition in an air environment. Decomposition takes place at the following temperatures: hemicellulose – (200–260) °C; cellulose – (240–350) °C; lignin – (280–500) °C [45].

It may be seen that DTA and TG curves of all specimens have two endothermal effects at temperature intervals of (80–200)°C and (700–800)°C, and one broad complex of inconspicuous exothermal effects at a temperature interval of (200–480)°C. The DTA curves of specimens with CM have an endothermal effect at a temperature range of (480–520)°C, which is attributed to the decomposition of P. We can observe that during the DTA/TG test, FHS exothermal effects end a little earlier than the start of decomposition in the cement minerals. So we can presume that the decomposition of FSH has a minor effect on the DTA/TG of cement minerals.

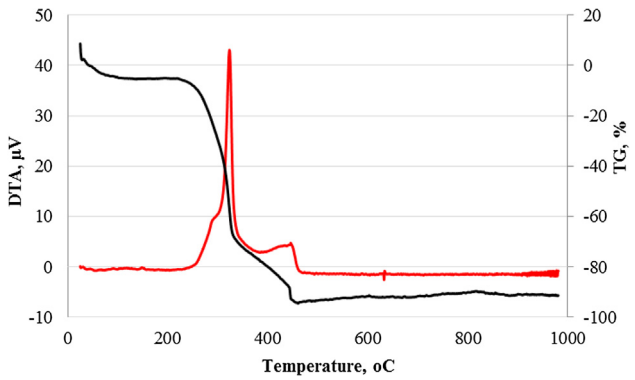

Fig. 5. DTA (red) and TG (black) curves of HS aggregate. (For interpretation of the references to colour in this figure legend, the reader is referred to the web version of this article.)

Normally, during the endothermic effect at a temperature interval of (30–105) °C the unbound and a part of the bound water are removed. The evaporable water is completely eliminated at 120 °C [40,41]. At a temperature of (100–200) °C, most of the cement mineral hydrates (calcium hydroaluminates, E, monocarboaluminates [42–44] etc.), lose hydrated water and during the endothermic effect (700–800) °C decomposition of C [45] is observed. The complex of exothermal effects may be attributed to the decomposition process of FHS. Mass losses of specimens with mineralized and non-mineralized aggregate (control) obtained via the TG method are presented in Table 4.

The mass loss of unbound water for the 28-day control specimen (up to 100 °C) is 1.50% (Fig. 9). Such a low mass loss is due to intensive water evaporation during the 28-day storage. It is assumed that a considerable endothermic effect with the mass loss of 3.4% obtained at 125 °C arises due to decomposition of E. This hypothesis is confirmed by XRD analysis and results presented in the literature [43,46]. At a temperature interval of (155–165)°C, a minor endothermic effect is observed with 1% of mass loss, and this may be attributed to loss of water from part of the carboaluminate hydrates [46]. At a temperature of (160–200) °C, there is a loss of bound water from the decomposition of the CSH [47], and TG analysis of the 28-day control specimen shows only 0.38% of mass loss, i.e. a minimum of CSH is formed. During the exothermal effect (two exothermal maximums at 300 °C and 465 °C), the control specimen loses 3.64% of its weight due to decomposition of cellulose and lignin from the FHS. Decomposition of P in DTA and TG is not observed. During decomposition of carbonates (700–800) °C, the specimen loses 1.04% of its weight. The overall mass loss is 12.94%.

TG data up to 100 °C for the 1-year control specimen shows 1.19% of mass loss. Comparing TG data for 28-day and 1-year control specimens, the tendencies of endothermic and exothermal effects are the same; except for the effect due to decomposition of carbonates i.e. the mass loss is higher (1.20%) for 1-year specimens. This is confirmed by XRD, where it can be seen that the intensity of the C peak is increased. Overall mass loss after 1 year is 11.36%.

In the DTA and TG curves for the 28-day composites with CM, a higher amount of unbound water is observed, whereas active water evaporation does not occur from the control specimen during 28 days. For compositions with mineralised aggregates, the mass loss of specimens (at temperature up to 100 °C) varies from 2.12% to 2.56%. The maximum temperature of the endothermal effect in the control specimen is 121 °C, while in compositions with didejanciu AS/CEM ratio are 127 °C, 130 °C and 140.3 °C respectively. It is possible that, due to the higher amount of AS in CM, more E and monosulphoaluminate are formed, and therefore, the displacement of the endothermal effect is at a higher temperature. At a temperature interval of (100–160)°C, the mass loss of the specimen increases with the increasing AS/CEM ratio in composition, and varies from 8.5% to 10.1%. Specimens with CM are characterised by a 4–6 times higher amount of CSH, and their mass loss

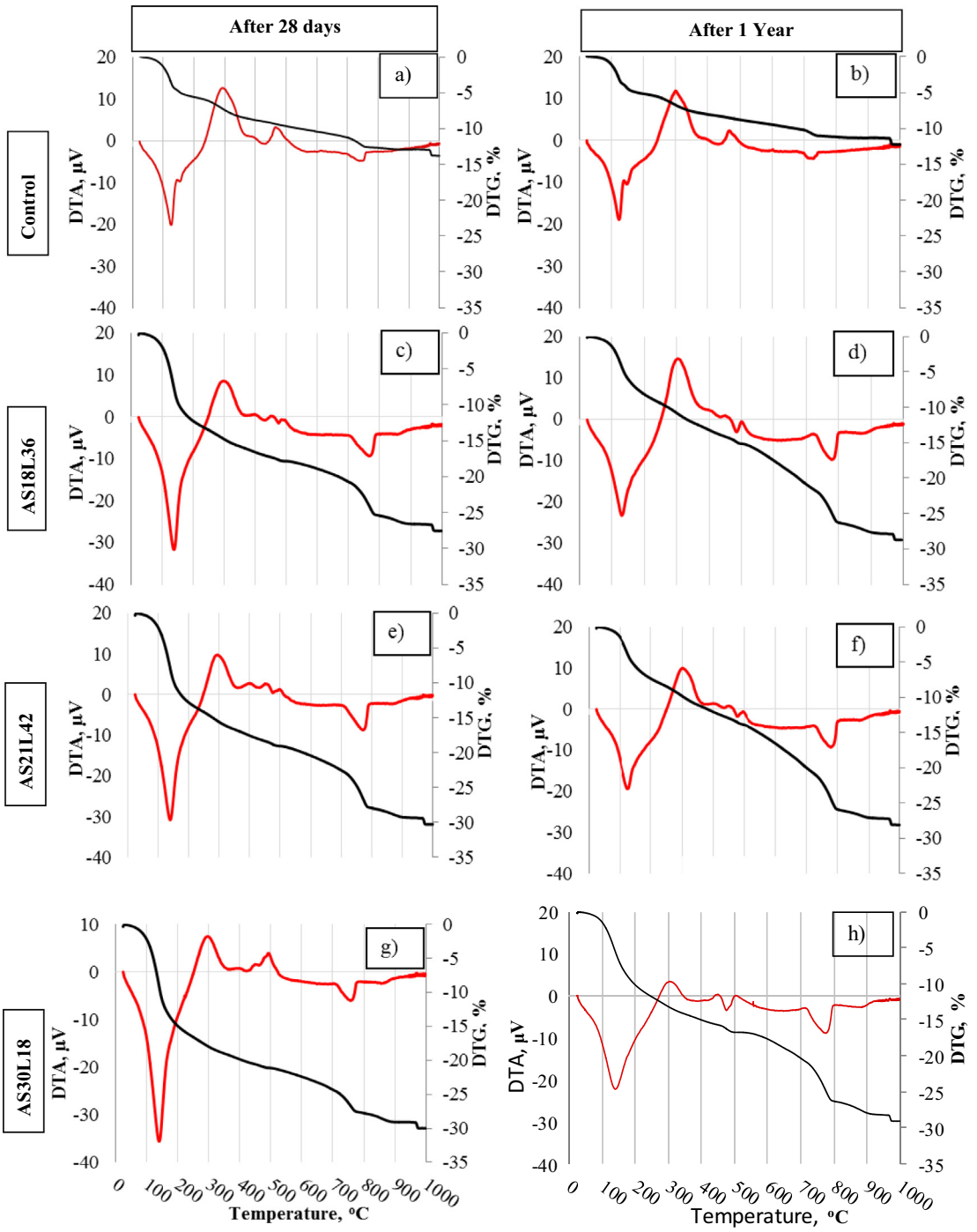

Fig. 6. DTA (red) and TG (black) curves of a composite matrix. (For interpretation of the references to colour in this figure legend, the reader is referred to the web version of this article.)

Table 4
Percentage mass losses determined during the TG test.

	Control		AS18L36		AS21L42		AS30L18	
	28 days	1 year	28 days	1 year	28 days	1 year	28 days	1 year
Up to 100 °C	1.50	1.19	2.12	1.54	2.15	1.44	2.56	1.64
Ettringite 100–160 °C	3.63	3.61	8.47	5.16	8.69	4.55	10.82	6.33
CSH 160–200 °C	0.38	0.41	1.85	1.55	2.06	1.33	2.46	2.35
Combustion 200–460 °C	3.635	3.31	6.2	6.12	5.84	5.80	5.86	5.61
Portlandite 480–550 °C	–	–	1.65	1.86	0.90	1.20	0.60	1.10
Carbonates 720–790 °C	1.04	1.20	5.50	5.8	5.0	5.9	4.0	5.76
Final	12.94	11.36	26.69	26.65	29.4	28.91	29.6	29.49

varies from 1.82% to 2.46% compared to the mass loss of the control specimen (0.38%). This means that a higher AS/ CEM ratio promotes not only the formation of E but also of CSH.

An assumable, broad exothermal effect is visible in all the compositions, with the maximum at 300 °C, which is obtained due to combustion residues of FHS. During combustion, the specimens with CM lose approximately two times more mass, i.e. (5.82–6.20)% compared to the control specimen (3.64%). One of the reasons why a higher mass loss in specimens with CM is obtained, is that the CM fixes calcium ions on the FHS surface, thus forming a stable calcium–pectin gel complex, holding up moisture [47,48], therefore, the degradation of hemicellulose and pectins occurs at a higher temperature (335 °C). Another reason is due to the formation of insoluble $Al(OH)_3$ on the FHS surface. When AS reacts with OH^- ions during the mineralization procedure, insoluble $Al(OH)_3$ fills the pores and gaps in the FHS. Its decomposition temperature is in the range of (220–300)°C and contributes to mass loss in the specimens.

It is likely that a few insignificant exothermal effects in the thermograms at a temperature range of (350–440)°C are obtained due to burning/incense of the cellulose and lignin in the FHS. The decomposition peaks of P in 28-day specimens show that the most of the P is formed in composition with the lowest AS/CEM ratio (AS18L36), where the pH value supposedly is higher. It can be assumed that this effect determines the highest strength properties of this composite. The highest AS/CEM ratio lowers the pH value in the composite, which is why the composition AS21L42 has 30%, and composition AS30L18 even 60%, less P than the composition with the lowest AS/CEM ratio. This means that the less AS is added, the more P is formed.

During decomposition of carbonates, the mass loss of specimens with CM is from 4 to 5 time higher than that of the control specimens (from 4% to 5.5% and ~1% respectively). It is assumed that the higher the amount of L used in CM, the higher the carbonation rate occurring during a long-term period. Whereas when CM is not used, no P forms, resulting in a lower amount of carbonates.

Overall mass losses of specimens with CM are at least two times greater compared to the control specimen. This shows that CM assures more intensive hydration of cement and the forming of a stable calcium–pectin gel complex. Therefore, compared to the control specimen (where active evaporation of water occurs at room temperature), water evaporation in specimens with CM at room temperature and under heating is significantly complicated.

After 1 year, evaporation of unbound water decreases and the mass loss at temperatures of up to 100 °C reduces in all specimens. The mass loss reduces at a temperature range of (100–160)°C due to the transformation of E, and at a temperature interval of (160–200) °C as well. During the exothermal effect, specimens that have been hardened for 1 year lose a relatively low amount of mass, which means that CM sufficiently covers the surface of the FHS and, during hardening, removal of water from the FHS is complicated. The decomposition peaks of P show that its amount in specimens is increased by (20–40)%. Mass loss due to the decomposition of carbonates in specimens significantly increases, up to 47% in specimens with the highest AS/CEM ratio. It may be assumed that this effect is obtained due to the decomposition of carbonates additionally formed during E transformation. The overall mass losses in specimens with lower AS/CEM ratio decrease from 29.49% to 26.65% respectively.

3.3. Density

It was found that the density of specimens after 28 days of curing varies from 779 kg/m^3 (control composition) to 863 kg/m^3 (AS18L36 composition) (Fig. 8), i.e. from 1.54% to 11%. The highest average density value is obtained for composites with lower AS/CEM ratios (AS18L36 and AS12L42). It is possible that the reduction of density in composites with the highest AS/CEM ratio can be attributed to a high amount of E, whose formation is caused by a high amount of AS during the mineralization process. The density of all 1-year composites is higher than that of the 28-day composites (Fig. 7).

The highest density growth (4.52%) during 1 year is obtained for AS21L42 specimens having the highest L/CEM ratio. This ensures a more intensive carbonation process and the formation of new intermediates (mostly vaterite) determining denser structure. The lowest density growth (3.22%) is obtained for the control specimen, due to the inhibition of the hydration process.

3.4. Compressive stress

When comparing the densities of the control specimen with specimens where mineralised FHS was used, it can be clearly seen that the density growth is quite low (10.8%, 8.8% and 1.5%), and the growth of the compressive strength is a lot higher (4.5, 3.9 and 2.1 times). These differences can be explained by the difference in the hydration products, because hydration in the composite with non–mineralized FHS (control composition) is strongly inhibited; portlandite formation does not occur, and only ettringite and CSH are present. A higher AS/CEM ratio determines more intensive formation of ettringite, whereas a lower ratio promotes the intensive formation of portlandite and CSH in the specimen. The highest compressive strength in the composite matrix can be caused by the highest P/E ratio and CSH amount, which are identified during XRD patterns analysis. We can observe that increasing the AS/CEM ratio in compositions after 28 days of curing determines the reduction of compressive strength from 8.03 MPa to 6.03 MPa (Fig. 8).

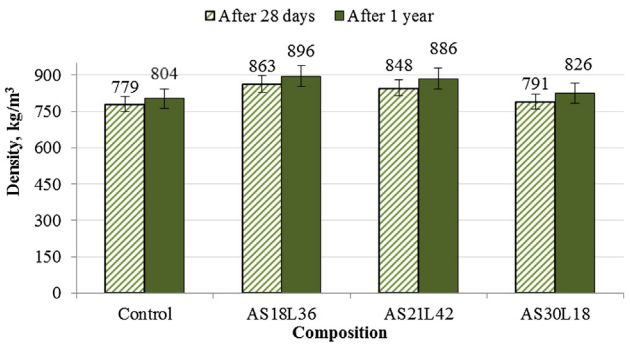

Fig. 7. Density of 28-day and 1-year composites.

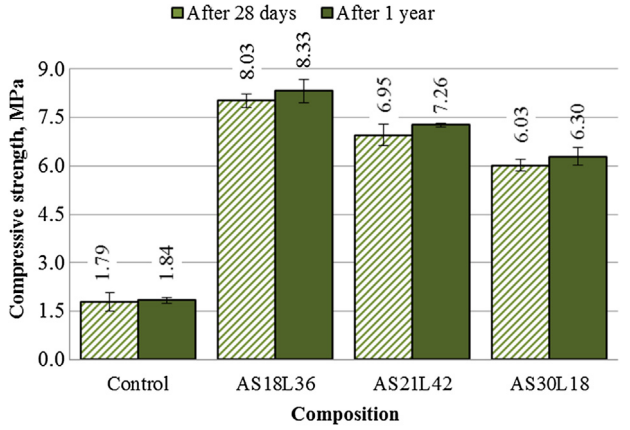

Fig. 8. 28-day and 1-year compressive strength of composites.

After 1 year of curing, the compressive strength for all compositions is increased from 2.8% to 4.5%. The higher strength increase is obtained for the compositions with CM. As XRD analysis shows, the increase in P is observed for the above-mentioned compositions. According to the compressive strength results we obtained, such composites can be used for building elements (for example blocks) suitable for installing bearing structures in low-rise buildings or as self-bearing elements in multi-storey buildings.

3.5. Microstructure after 28 days and 1 year.

Fig. 9 presents the matrix microstructure of 1-year composites (magnification x3000).

As can be seen, the matrix of the control specimen is heterogeneous and has indefinite shapes. Large partially dissolved cement grains as well as newly formed intermediates are observed. It can be seen that there are a large number of cavities between non-hydrated cement grains, and empty cavities remain due to the evaporation of unbound water, which is confirmed by TG tests. The above-mentioned cavities cause lower density and mechanical properties. Fig. 9b shows that the densest matrix is obtained for the AS18L36 specimen. It is homogeneous, and spaces between the cement grains are a lot smaller. Apparently, the denser microstructure of the composite determines the highest mechanical properties. The microstructure of the AS21L42 matrix (Fig. 9c) is also sufficiently dense, and spaces between grains are covered with newly formed intermediates. Compare to the control specimen, finer grains of cement minerals are seen in the AS30L18 matrix. It may be assumed that the grains are partially dissolved, and this is confirmed by the accumulation of fine newly formed intermediates on the cement grains; however, these intermediates do not form a homogeneous matrix. The general view of the matrix is slightly similar to that of the control specimen.

3.6. Thermal conductivity

Comparing the thermal conductivity values of 28-day and 1-year specimens, it may be noticed that the thermal conductivity of all composites increases during long-term curing. The increase in thermal conductivity (Fig. 10) is probably caused by density growth.

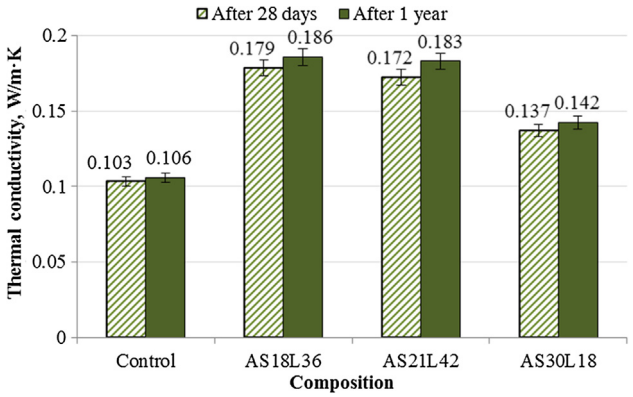

Fig. 10. Thermal conductivity of 28-day and 1-year composites.

The lowest increase in thermal conductivity is obtained for the control specimen and the highest – for the AS21L42 specimen. Apparently, more hydration products are formed in this specimen during cement hydration when a higher amount of lime exists, and more hydrates participate in the carbonation process. As a result, a denser structure is obtained, which causes higher heat transfer by conduction.

4. Conclusions

After 28 days of curing, the CM promotes in mineralized specimens with FSH a stable calcium–pectin gel complex forming on the surface of the FHS, thus assuring more intensive cement hydration and the formation of various hydration products. The higher AS/CEM ratio in mineralized specimens determines more intensive formation of ettringite, whereas a lower ratio promotes intensive formation of portlandite and CSH. In the non–mineralized specimen (control composition), the hydration process is strongly inhibited, and only ettringite and CSH are present. In 1-year cured composites, the peak intensity of ettringite reduces, while the peak

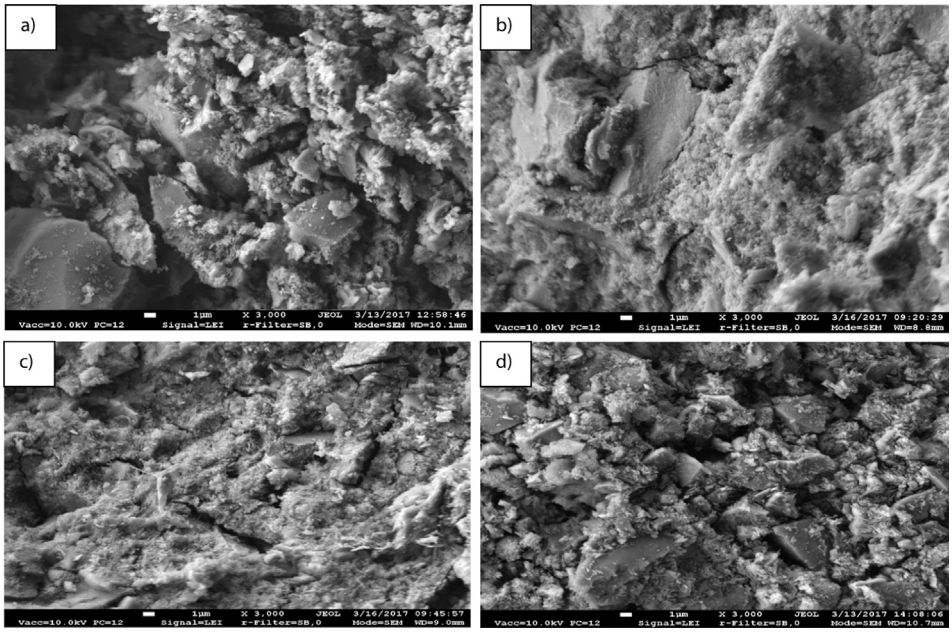

Fig. 9. Structure of composite matrices at a magnification of x3000. (a) – Control specimen; (b) – AS18L36 specimen; (c) – AS21L42 specimen; (d) – AS30L18 specimen.

intensity of calcite (except for the composition AS30L18 with the highest AS/CEM ratio), CSH and portlandite increases. The lower AS/CEM ratio and respectively higher L/CEM ratio in compositions (AS18L36 and AS21L42) lead to the formation of vaterite. When the AS/CEM ratio is the highest (AS30L18), vaterite does not occur.

The overall mass losses of specimens with CM during TG tests are at least two times greater (by 2–2.2 times after 28 days and by 2.4–2.5 times higher after 1 year) compared to the control specimen, because when the AS/CEM ratio increases in compositions, mass losses increase due to the following:

the evaporation of unbound water – from 40 to 45% after 28 days, and 21–38% after 1 year; ettringite decomposition – from 2.3 to 2.8 times after 28 days, and 26–75% higher after 1 year; CSH – from 4.8 to 6.5 times after 28 days, and from 3.2 to 5.7 times higher after 1 year; organic compounds – from 70% to 60% after 28 days, and from 87% to 69% higher after 1 year; portlandite – from 1.5% to 0.6% after 28 days, and from 1.76% to 1.1% higher after 1 year; carbonates – from 5.5 to 3.85 times after 28 days, and from 4.45 to 4.7 times higher after 1 year.

The higher hydrated lime amount in CM provides an alkaline environment and intense cement hydration, which is why the highest average densities, equal to 863 kg/m^3 and 848 kg/m^3, are obtained for composites with lower AS/CEM ratios. The highest AS/CEM ratio (AS30L18) determines lower density, which is 791 kg/m^3, possibly due to the higher AS content, providing an acidic environment, and promotes ettringite formation. The highest L/CEM ratio in a composition ensures a more intensive carbonation process, denser structure formation and the highest increase in density during 1 year of curing. The lowest increase in density (3.22%) is obtained for the control specimen due to inhibition of the hydration process.

In comparison to the control composition, an increase in the AS/CEM ratio in compositions leads to an increase in compressive strength for 28-day specimens by 4.5, 3.9 and 2.1 times. The highest compressive strength is caused by the highest P/E ratio and CSH amount in the composite. The highest increase in compressive strength during 1 year, which is equal to 4.5%, is observed for the compositions with a higher AS/CEM due to the P/E ratio increasing.

The lowest increase in thermal conductivity in 1-year specimens is obtained for the control specimen, characterized by the lowest density. The highest increase in thermal conductivity is obtained for the mineralized compositions, especially for the AS21L42 composition with the highest density and the highest L/CEM ratio, which ensures the participation of more hydrates in the carbonation process leading to a denser composite structure and higher heat transfer by conduction.

Conflict of interest

None.

Acknowledgment

The authors gratefully acknowledge Vilnius Gediminas Technical University Civil Engineering Scientific Research Centre for providing the laboratory equipment used in the present investigation.

This research did not receive any specific grant from funding agencies in the public, commercial or not-for-profit sectors.

References

[1] M. Karus, D. Vogt, European hemp industry: cultivation, processing and product lines, Euphytica 140 (2004) 7–12, https://doi.org/10.1007/s10681-004-4810-7.
[2] E. Sassoni, S. Manzi, A. Motori, M. Montecchi, M. Canti, Novel sustainable hemp-based composites for application in the building industry: physical, thermal and mechanical characterization, Energy Build. 77 (2014) 219–226, https://doi.org/10.1016/j.enbuild.2014.03.033.
[3] P.B. de Bruijn, K.H. Jeppsson, K. Sandin, C. Nilsson, Mechanical properties of lime–hemp concrete containing shives and fibres, Biosyst. Eng. 103 (2009) 474–479, https://doi.org/10.1016/j.biosystemseng.2009.02.005.
[4] Diquélou, E. Gourlay, L. Arnaud, B. Kurek, Impact of hemp shiv on cement setting and setting: influence of the extracted components from the aggregates and study of the interfaces with the inorganic matrix, Cem. Concr. Compos. 55 (2015) 112–121, https://doi.org/10.1016/j.cemconcomp.2014.09.004.
[5] S. Elfordy, F. Lucas, Tancret, Y. Scudeller, L. Goudet, Mechanical and thermal properties of lime and hemp concrete (“hempcrete”) manufactured by a projection process, Constr. Build. Mater. 22 (2008) 2116–2123, https://doi.org/10.1016/j.conbuildmat.2007.07.016.
[6] Edward A.J. Hirst, P. Walker, K.A. Paine, T. Yates, Characteristics of low-density hemp-lime building materials 2012, 165(1), 165, 15–23. doi: 10.1680/coma.1000021.
[7] F. Collet, J. Chamoin, S. Pretot, C. Lanos, Comparison of the hygric behaviour of three hemp concretes, Energy Build. 62 (2013) 294–303, https://doi.org/10.1016/j.enbuild.2013.03.010.
[8] P. Daly, P. Ronchetti, T. Woolley, Hemp Lime Bio-Composite as a Construction Material, Environmental Protection Agency, Ireland, 2010.
[9] P. Glé, E. Gourdon, L. Arnaud, Acoustical properties of materials made of vegetable particles with several scales of porosity, Appl. Acoust. 72 (2011) 249–259, https://doi.org/10.1016/j.apacoust.2010.11.003.
[10] L. Arnaud, E. Gourlay, Experimental study of parameters influencing mechanical properties of hemp concretes, Constr. Build. Mater. 28 (2012) 50–56, https://doi.org/10.1016/j.conbuildmat.2011.07.052.
[11] Y. Diquélou, E. Gourlay, L. Arnaud, B. Kurek, Influence of binder characteristics on the setting and setting of hemp lightweight concrete, Constr. Build. Mater. 112 (2016) 506–517, https://doi.org/10.1016/j.conbuildmat.2016.02.138.
[12] D. Fengel, Wengener G. Wood, Chemistry, Ultrastructure, Reaction, 1984, 613. doi: 10.1002/pol.1985.130231112.
[13] M. Bołtryk, E. Pawluczuk, Properties of a lightweight cement composite with an ecological organic filler, Constr. Build. Mater. 51 (2014) 97–105, https://doi.org/10.1016/j.conbuildmat.2013.10.065.
[14] G. Balčiūnas, I. Pundienė, L. Lekunaitė-Lukošiūnė, S. Vėjelis, A. Korjakins, Impact of hemp shives aggregate mineralization on physical-mechanical properties and structure of composite with cementitious binding material, Ind. Crops Prod. 77 (2015) 724–734, https://doi.org/10.1016/j.indcrop.2015.09.011.
[15] N.B. Milestone, Hydration of tricalcium silicate in the presence of lignosulfonates, glucose, and sodium gluconate, J. Am. Ceram. Soc. 62 (7–8) (1979) 321–324, https://doi.org/10.1111/j.1151-2916.1979.tb19068.x.
[16] D.P. Miller, A.A. Moslemi, Wood–cement composites: effect of model compounds on hydration characteristics and tensile strength, Wood Fiber Sci. 23 (4) (1991) 472–482.
[17] S. Frybort, R. Mauritz, A. Teischinger, U. Muller, Cement bonded composites – a mechanical review, BioResources 3 (2) (2008) 602–626.
[18] W.Y. Ahn, The effect of calcium chloride and D-Glucoses on surface hydration of Portland cement paste and morphological changes of hydrates, J. Natl. Acad. Sci. 20 (1981) 209–225.
[19] J. Fergusson, R. Hart, CXC Chemistry. 1958:509. ISBN 0199142440.
[20] F. Laoutid, M. Lorgouilloux, L. Bonnaud, D. Lesueur, P. Dubois, Fire retardant behaviour of halogen-free calcium-based hydrated minerals, Polym. Degrad. Stabil. 136 (2017) 89–97, https://doi.org/10.1016/j.polymdegradstab.2016.12.013.
[21] M. Le Troëdec, P. Dalmay, C. Patapy, C. Peyratout, A. Smith, T. Chotard, Mechanical properties of hemp-lime reinforced mortars: influence of the chemical treatment of fibers, J. Compos. Mater. 47 (22) (2011) 2347–2357, https://doi.org/10.1177/0021998311401088.
[22] N. Ševulová, E. Terpáková, J. Čigášová, J. Junák, L. Kidalová, Chemically treated hemp shives as a suitable organic filler for lightweight composites preparing, Proc. Eng. 42 (2012) 948–954.
[23] J. Salas, M. Alvarez, J. Veras, Lightweight insulating concretes with rice husk, Int. J. Cem. Compos. Lightweight Concr. 8 (1986) 171–180.
[24] M. Chabannes, E. Garcia-Diaz, L. Clerc, J.L. Bénézet, Effect of curing conditions and $Ca(OH)_2$-treated aggregates on mechanical properties of rice husk and hemp concretes using a lime-based binder, Constr. Build. Mater. 102 (2016) 821–833, https://doi.org/10.1016/j.conbuildmat.2015.10.206.
[25] EN 1990: Eurocode – Basis of structural design.
[26] M.A.A. Abd elaty, Compressive strength prediction of Portland cement concrete with age using a new model, HBRC J. 10 (2013) 145–155, https://doi.org/10.1016/j.hbrcj.2013.09.005.
[27] A. Çolak, A new model for the estimation of compressive strength of Portland cement concrete, Cem. Concr. Res. 36 (2006) 1409–1413, https://doi.org/10.1016/j.cemconres.2006.03.002.
[28] I.G. Richardson, The calcium silicate hydrates, Cem. Concr. Res. 38 (2) (2008) 137–158, https://doi.org/10.1016/j.cemconres.2007.11.005.
[29] L. Zhang, L.J. Catalan, R.J. Balec, A.C. Larsen, H.H. Esmaeili, S.D. Kinrade, Effects of saccharide set retarders on the hydration of ordinary Portland cement and pure tricalcium silicate, J. Am. Ceram. Soc. 93 (1) (2010) 279–287, https://doi.org/10.1111/j.1551-2916.2009.03378.x.
[30] L. Zhang, J.J. Lionel, L.J.J. Catalan, C. Andrew, A.C. Larsen, D. Stephen, S.D. Kinrade, Effects of sucrose and sorbitol on cement-based stabilization/solidification of toxic metal waste, J. Hazard. Mater. 151 (2008) 490–498, https://doi.org/10.1016/j.jhazmat.2007.06.022.

[31] M. Collepardi, S. Monosi, G. Moriconi, M. Pauri, Influence of gluconate, lignosulfonate, and glucose admixtures on the hydration of tetracalcium aluminoferrite in the presence of gypsum with or without calcium hydroxide, J. Am. Ceram. Soc. 68 (5) (1985) 126–128, https://doi.org/10.1111/j.1151-2916.1985.tb15330.x.
[32] M. Bishop, A.R. Barron, Cement hydration inhibition with sucrose, tartaric acid, and lignosulfonate: analytical and spectroscopic study, Ind. Eng. Chem. Res. 45 (2006) 7042–7049, https://doi.org/10.1021/ie060806t.
[35] H.F.W. Taylor, Cement Chemistry. 1997, 480 p. ISBN 0 7277 2592 0.
[36] P. Jiahui, Z. Jianxin, Q. Jindong, The mechanism of the formation and transformation of ettringite, 2006, 21(3), 158–161. doi: 10.1007/BF02840908.
[37] S.M. Shin, S. Ho Ch, Y. Sh. Song, J.P. Lin, Kinetics of the reaction of Ca(OH)2 with CO2 at low temperature, Ind. Eng. Chem. Res. 38 (4) (1999) 1316–1322, https://doi.org/10.1021/ie980508z.
[38] B. Vekteris, V. Vilkas, Betono tvarumas: Betono sulfatinė ir šarminė korozija, atsparumas šalčiui ir karbonizacijai. Tyrimai ir prevencinės priemonės: Monografija. ENG.: Stability of concrete: monograph, 2006, 162, ISBN: 9955251581.
[39] M.R. Hartmann S.K. Brady R. Berliner M.S. Conradi The evolution of structural changes in ettringite during thermal decomposition J. Solid State Chem. 179 2006 1259 1272 0.1016/j.jssc.2006.01.038
[40] W. Sha, E.A. O'Neill, Z. Guo, Differential scanning calorimetry study of ordinary Portland cement, Cem. Concr. Res. 29 (9) (1999) 1487–1489, https://doi.org/10.1016/S0008-8846(99)00128-3.
[41] R. Gabrovšek, T. Vuk, T. Kaučič, The preparation and thermal behavior of calcium monocarboaluminate, Acta Chim. Slovenica 55 (4) (2008) 942–950.
[42] Q. Zhou, F.P. Glasser, Thermal stability and decomposition mechanisms of ettringite at <120 degrees C, Cem. Concr. Res. 31 (9) (2001) 1333–1339, https://doi.org/10.1016/S0008-8846(01)00558-0.
[43] E. Nonnet, N. Lequeux, P. Boch, Elastic properties of high alumina cement castables from room temperature to 1600°C, J. Eur. Ceram. Soc. 19 (8) (1999) 1575–1583, https://doi.org/10.1016/S0955-2219(98)00255-6.
[44] E.T. Stepkowska, Simultaneous IR/TG study of calcium carbonate in two aged cement pastes, 2006, 84(1), 175–180. doi: 10.1007/s10973-005-7179-5.
[45] A.F. Roberts, A review of kinetic data for the pyrolysis of wood and related substances, Combust. Flame 14 (1970) 261–272.
[46] G.A. Khoury, Compressive strength of concrete at high temperatures: a reassessment, 1992, 44(161), 291–309. doi: 10.1680/macr.1992.44.161.291.
[47] M.L. Troëdec, P. Dalmay, C. Patapy, C. Peyratout, A. Smith, T. Chotard, Mechanical properties of hemp-lime reinforced mortars: influence of the chemical treatment of fibers, J. Compos. Mater. 45 (22) (2011) 2347–2357, https://doi.org/10.1177/0021998311401088.
[48] M.L. Troëdec, D. Sedan, C. Peyratout, C. Peyratout, J.P. Bonnet, A. Smith, R. Guinebretiere, V. Gloaguen, P. Krausz, Influence of various chemical treatments on the composition and structure of hemp fibres, Compos. Part A Appl. Sci. Manuf. 39 (3) (2008) 514–522, https://doi.org/10.1016/j.compositesa.2007.12.001.
[49] S. Pantawee, Th. Sinsiri, Ch. Jaturapitakkul, P. Chindaprasirt, Utilization of hemp concrete using hemp shiv as coarse aggregate with aluminium sulfate [$Al_2(SO_4)_3$] and hydrated lime [$Ca(OH)_2$] treatment, Constr. Build. Mater. 156 (2017) 435–442, https://doi.org/10.1016/j.conbuildmat.2017.08.181.